

Ab Initio Free Energy Surfaces for Coupled Ion-Electron Transfer

Ethan Abraham*

Department of Chemistry, Massachusetts Institute of Technology, Cambridge, Massachusetts 02139, USA

Martin Z. Bazant

*Department of Chemical Engineering, Massachusetts Institute of Technology, Cambridge, Massachusetts 02139, USA and
Department of Mathematics, Massachusetts Institute of Technology, Cambridge, Massachusetts 02139, USA*

Troy Van Voorhis

Department of Chemistry, Massachusetts Institute of Technology, Cambridge, Massachusetts 02139, USA

(Dated: October 27, 2025)

The Marcus theory of electron transfer assumes that diabatic energy gaps are sampled from a single ensemble. This assumption can break down in spatially anisotropic environments, such as electrochemical interfaces or biomolecular structures, where distinct solvent ensembles arise along a collective variable describing the anisotropy. Treating this collective variable as an additional reaction coordinate linearly independent from the Marcus reaction coordinate, we develop a formalism that enables calculation of the resulting Coupled Ion–Electron Transfer (CIET) free-energy surface directly from constrained *ab initio* trajectories. Applied to CO₂ redox on a gold electrode, this method reveals strong coupling to the anisotropy, predicting significantly different activation barriers compared to either coordinate alone.

Marcus free energy curves relate macroscopically observed electron transfer (ET) reaction rates to a microscopic picture of solvent fluctuations [1–3]. The iconic parabolic free energy curves that describe the ET landscape arise from the fact that the energy gap between the reactant and product diabatic electronic states is mediated by the instantaneous nuclear configurations of the solvation environment, and that the probability distribution of such energy gaps is Gaussian to a good approximation; taking the logarithm of this distribution yields the parabolas [4–6]. Crucially, this framework assumes that nuclear configurations are sampled from a single, global equilibrium ensemble—a simplification that may break down in anisotropic environments such as electrochemical interfaces or biomolecular structures [7–10].

In this Letter, we show that in the presence of such anisotropy, ET can become coupled to a classical collective variable (CV) that characterizes the broken symmetry. This is suggested by the fact that the nuclear ensembles, when conditioned on different values of the CV, are generally distinct. As a result, the Marcus curves associated with each value may differ in curvature or vertical shift, and the reaction landscape is more appropriately viewed as a 2D manifold of Marcus curves parametrized by the anisotropic CV.

Extensions of Marcus theory to cases in which ET is coupled to another degree of freedom have already found widespread applications. Proton-coupled electron transfer (PCET) generalizes Marcus theory by extending the reaction coordinate to include a proton degree of freedom [9, 10]. However, the proton is typically treated quantum mechanically and associated with a reaction coordinate involving vibronic excitations, precluding a straightforward generalization to the case when ET is coupled to a classical CV. More

recently, coupled ion-electron transfer (CIET), proposed by Bazant and coworkers [7, 8], has emerged as a framework to explain the rates of redox reactions in commercial lithium-ion battery electrodes [11, 12]. In this theory, the Marcus ET coordinate is coupled to a classical ion transfer (IT) coordinate related to the distance from the electrode–electrolyte interface, and the resulting rate expressions fit the experimentally observed current-voltage curves better than rate expressions that do not take into account ion-electron coupling [7, 12, 13].

Despite the emergence of Marcus theory in recent decades as a physically correct way to view ET reactions, the Butler–Volmer (BV) equation, which has empirically expressed Tafel’s law for current-voltage relationships of reaction-limited currents for nearly a century, assumes diabatic free energy curves that are linear instead of quadratic [14, 15]. In CIET, this discrepancy is resolved by postulating a 2D free energy surfaces which can in general have an arbitrary structure, but in the simplest approximation is linear when cross-sectioned along the ion-transfer CV and quadratic along the Marcus ET coordinate [7]. The result is that the CIET rate expression reduces to the Marcus–Hush–Chidsey (MHC) equation [16–18] in the limit where the reorganization energy dominates, and reduces to the BV equation in the limit where the barrier along the classical IT coordinate dominates [7]. The fact that viewing an electron transfer reaction as coupled to an anisotropic CV not only explains experimental reaction rates but also unifies physical equations correct in different regimes suggests the utility of such an approach, and suggests the possibility that a related framework can be generalized to symmetry-broken CVs other than IT at intercalation cathodes, finding broader applications across condensed phase physical chemistry [19, 20]. Practical analyses using these multidimensional surfaces may also become more feasible with concurrent improvements in sampling methods and machine-learned potentials [21–26].

* ethana@mit.edu

We note that *ab initio* computation of CIET parameters has recently been explored by Stenlid *et al.* on a model lithium-cobalt-oxide battery interface [11]. While their reported parameters reproduced trends observed in experimental current-voltage relationships, we noticed several key methodological inconsistencies in their study (see Supplementary Material for details). Here we present the first physically consistent formalism to compute finite-temperature 2D free-energy surfaces for ET coupled to a classical CV, expressed entirely in terms of quantities derived from constrained *ab initio* trajectories. We incorporate adiabatic corrections to the landscape as well, which prove to be significant [16]. We illustrate the method by applying it to CO₂ redox on a gold electrode, and we find that the transition state (TS) of the 2D landscape can be significantly lower than when computed from the ET coordinate or CV alone. Although this demonstration assumes harmonic and symmetric ET, the framework allows this assumption to be readily relaxed, enabling generalization to diverse systems.

Constructing the 2D Free Energy Surface. Within the Born–Oppenheimer approximation, an *ab initio* trajectory constrained to a diabatic electronic state can be modeled using constrained density functional theory (cDFT), as developed by Van Voorhis and co-workers [27–29] and implemented in various software packages [30–32]. Consider a simulation of N atoms with the electronic state fixed to $|\alpha\rangle = |\alpha(\mathbf{R})\rangle$, where $\mathbf{R} \in \mathbb{R}^{3N}$ denotes the nuclear configuration. Let $\mathbf{R}_\alpha(t)$ denote the nuclear trajectory under this constraint. At steady state, the probability of finding the system in configuration \mathbf{R} is given by the time-independent distribution $p_\alpha(\mathbf{R})$. Letting $\alpha = O, R$ denote the initial and final (i.e. oxidized and reduced) diabatic states of the electron transfer, the ET coordinate of \mathbf{R} is defined by the energy gap [4, 33, 34]

$$q(\mathbf{R}) = \langle O(\mathbf{R}) | \hat{H} | O(\mathbf{R}) \rangle - \langle R(\mathbf{R}) | \hat{H} | R(\mathbf{R}) \rangle, \quad (1)$$

where \hat{H} is the Hamiltonian. Now suppose $\xi = \xi(\mathbf{R})$ is a CV that characterizes the anisotropy. Then the histogram $\mathcal{N}_\alpha(q, \xi)$ is obtained from the trajectory by integrating over the appropriate region of the phase space

$$\mathcal{N}_\alpha(q, \xi) = \int dt \int d^{3N} \mathbf{R} \delta(q(\mathbf{R}_\alpha(t)) - q) \delta(\xi(\mathbf{R}_\alpha(t)) - \xi). \quad (2)$$

The probability distribution is then given by $p_\alpha(q, \xi) = \mathcal{N}_\alpha(q, \xi) / \int dq d\xi \mathcal{N}_\alpha(q, \xi)$, and the 2D *excess* free energy [35] surface is given by

$$G_\alpha^{\text{ex}}(q, \xi) = -k_B T \ln p_\alpha(q, \xi) + C_\alpha, \quad (3)$$

where C_α is a constant. It is convenient when applicable to define the equilibrium coordinates for each state

$$(q_\alpha, \xi_\alpha) = \underset{q, \xi}{\text{argmax}} p_\alpha(q, \xi). \quad (4)$$

Then, noting that the constants C_O and C_R must be related such that the reaction free energy between these equilibrium states is the thermodynamic driving force $\Delta G_{OR}^{\text{ex}}$, a natural choice is

$$C_O = k_B T \ln p_O(q_O, \xi_O), \quad (5a)$$

$$C_R = \Delta G_{OR}^{\text{ex}} + k_B T \ln p_R(q_R, \xi_R) \quad (5b)$$

so that the equilibrium reactant state has $G_O^{\text{ex}}(q_O, \xi_O) = 0$.

A practical challenge is that in the presence of high reaction barriers, the sampled histogram $p_\alpha(q, \xi)$ is often unpopulated for many regions in the 2D reaction coordinate space including, crucially, near the TS. However, this challenge can easily be overcome by employing methods common in Marcus theory (for q) and classical enhanced sampling (for ξ). Sampling over the CV can be achieved by standard techniques such as metadynamics or harmonic restraints [21, 36, 37]. If $U_\alpha^{\text{bias}}(\xi)$ is the resulting bias potential, the true distribution $p_\alpha(q, \xi)$ can be obtained from the observed distribution via

$$p_\alpha(q, \xi) = p_\alpha^{\text{obs}}(q, \xi) \exp[+U_\alpha^{\text{bias}}(\xi)/k_B T]. \quad (6)$$

Once the ξ is sampled, the cross-sectional Marcus free energy curves are obtained by invoking the standard assumption that they are parabolic, whereby

$$p_\alpha(q|\xi) = \frac{1}{\sqrt{4\pi k_B T \lambda_\alpha(\xi)}} \exp\left(-\frac{(q - E_\alpha(q|\xi))^2}{4k_B T \lambda_\alpha(\xi)}\right), \quad (7a)$$

$$\lambda_\alpha(\xi) = \frac{\text{Var}_\alpha(q|\xi)}{2k_B T}. \quad (7b)$$

Here $E_\alpha(q|\xi)$ and $\text{Var}_\alpha(q|\xi)$ denote, respectively, the mean and variance of the conditional distribution $p_\alpha(q|\xi)$, which can be approximated from $p_\alpha^{\text{obs}}(q|\xi)$ [38].

In the standard case that the sampling is performed such that $p_\alpha^{\text{obs}}(\xi) = \int dq p_\alpha^{\text{obs}}(q, \xi)$ is constant, using Eq. (5)-(7), we now obtain for our free energy surfaces

$$G_O^{\text{ex}}(q, \xi) = -[U_O^{\text{bias}}(\xi) - U_O^{\text{bias}}(\xi_O)] + \frac{(q - E_O(q|\xi))^2}{4\lambda_O(\xi)}, \quad (8a)$$

$$G_R^{\text{ex}}(q, \xi, \Delta G_{OR}^{\text{ex}}) = -[U_R^{\text{bias}}(\xi) - U_R^{\text{bias}}(\xi_R)] + \frac{(q - E_R(q|\xi))^2}{4\lambda_R(\xi)} + \Delta G_{OR}^{\text{ex}}. \quad (8b)$$

In the demonstration presented below, we further simplify by assuming $\lambda_O(\xi) = \lambda_R(\xi) = \lambda$, only because the available sampling was insufficient to resolve any ξ -dependence from the statistical noise across runs. Nonetheless, we emphasize that the reorganization energy may, in general, be both asymmetric and depend on ξ . (Note we assume that both the ET and CV coordinates are overdamped, with the CV relaxing on a slower timescale than the ET coordinate, allowing $p_\alpha(q|\xi)$ to be obtained from enhanced sampling [19, 39]. These assumptions will be revisited in future work).

Finally, the free energy curves obtained via the above method can be used to compute the TS and activation barrier. The intersection of the curves is given by the set

$$\mathcal{J} = \{(q, \xi) : G_R^{\text{ex}}(\xi, q) = G_O^{\text{ex}}(q, \xi)\}, \quad (9)$$

and the TS and activation barrier in the non-adiabatic limit are given by

$$(\xi_\ddagger, q_\ddagger) = \underset{(q, \xi) \in \mathcal{J}}{\text{argmin}} G_O^{\text{ex}}(q, \xi), \quad (10a)$$

$$\Delta G_\ddagger^{\text{ex}} = G_O^{\text{ex}}(q_\ddagger, \xi_\ddagger). \quad (10b)$$

Adiabatic corrections to these values are discussed below.

For visualization and comparison of landscapes between systems, it is convenient to nondimensionalize both reaction coordinates. For the CV, the natural choice is

$$\tilde{\xi} = \frac{\xi - \xi_O}{\xi_R - \xi_O}, \quad (11)$$

where ξ_O and ξ_R are determined from Eq. (4) and the tilde denotes a nondimensionalized quantity. If we plot the CV and ET coordinates on perpendicular axes (see Supplementary Material for analysis of the coordinate orthogonality), and enforce that the initial and final Marcus parabolas in each cross section lie at 0 and 1 respectively, we obtain for the ET coordinate

$$\tilde{q}(\tilde{\xi}) = \frac{q - E_O(q|\tilde{\xi})}{E_R(q|\tilde{\xi}) - E_O(q|\tilde{\xi})}. \quad (12)$$

Note that the nondimensionalization scheme stretches the ET coordinate differently at different CV values. However, it can be easily seen that this transformation maps only the ranges of the reaction coordinates, and so barrier heights in Eq. (10b) are unaffected by the non-dimensionalization.

Once obtained, the activation barrier can be used to derive ET rate expressions. As in standard Marcus theory, we note that the thermodynamic free energy $\Delta G_{OR}^{\text{ex}}$, which determines the shift of the two diabatic surfaces relative to each other, can depend on factors such as electrochemical overpotential, which only weakly effect the shape of the individual surfaces. Thus $\Delta G_{\ddagger}^{\text{ex}} = \Delta G_{\ddagger}^{\text{ex}}(\Delta G_{OR}^{\text{ex}})$ can be obtained from Eq. (10) numerically, and the non-adiabatic rate expression for a discrete transition can be determined from Fermi's golden rule

$$k(\Delta G_{OR}^{\text{ex}}) = \frac{2\pi}{\hbar} |H_{OR}|^2 \mathcal{P}(\Delta G_{OR}^{\text{ex}}), \quad (13a)$$

$$\mathcal{P}(\Delta G_{OR}^{\text{ex}}) = Q^{-1} \exp[-\Delta G_{\ddagger}^{\text{ex}}(\Delta G_{OR}^{\text{ex}})/k_B T], \quad (13b)$$

where $Q = \int d\Delta G_{OR}^{\text{ex}} \exp[-\Delta G_{\ddagger}^{\text{ex}}(\Delta G_{OR}^{\text{ex}})/k_B T]$ is a partition function and $H_{OR} = \langle O|\hat{H}|R\rangle$ is the electronic coupling.

The rate expression for electron transfer where $|O\rangle$ is a discrete state and $\{|R\rangle\}$ is a continuum of states can be derived using a generalized MHC integral, integrating over the continuum

$$k = \frac{2\pi}{\hbar} |H_{OR}|^2 Q^{-1} \int d\varepsilon_R \rho(\varepsilon_R) n(\varepsilon_R) \exp\left(-\frac{\Delta G_{\ddagger}^{\text{ex}}(\Delta G_{OR}^{\text{ex}}, \varepsilon_R)}{k_B T}\right), \quad (14)$$

where ρ is the density of the continuum, n is the Fermi-Dirac occupancy, and G_{\ddagger} is now a function not only of some global shift $\Delta G_{OR}^{\text{ex}}$ but also the location of the final state's energy ε_R within the continuum.

We emphasize that the formalism presented up to this point is general, and the analytical CIET expressions of Ref. [7] can be derived upon specialization to certain electrochemical system and making the assumption that the free energy surfaces have a particular shape.

Example Application: CO₂ redox. The choice of the CO₂ redox system for demonstration of the above methodology is due to the relative simplicity of approximating the diabatic

states. Defining the diabatic states for lithium-ion intercalation, for example, is much more difficult because the lithium ion does not change its oxidation state during the intercalation process. Instead, the electrode is reduced to accommodate the lithium ion's charge, leading to diabatic states whose definition remains an open scientific question [12]. A simplified approach to this problem was adopted in Ref. [11] and will be extended in future work. Here, we instead demonstrate this Letter's methodology on the supposed rate-determining step of CO₂ reduction [40–42], where the diabatic states— $|\text{CO}_2\rangle$ and $|\text{CO}_2^-\rangle$ —are obtained via simple constraints, and where a CIET-like approach is less explored.

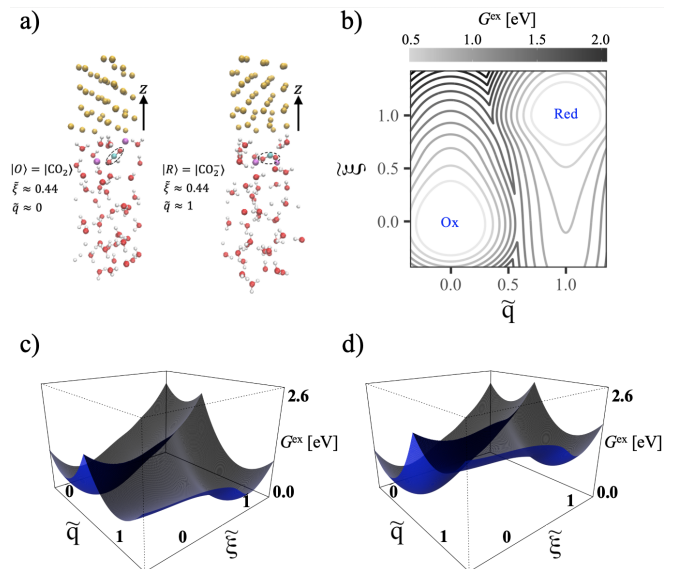


FIG. 1. Snapshots of the model aqueous CO₂-Au interface constrained to (left) the oxidized and (right) the reduced state. The circled CO₂ is linear in the oxidized state and bent in the reduced state. Au, C, O, H, and K are shown in gold, blue, red, white, and purple, respectively. The z -coordinate is taken normal to the electrode surface in the direction of the bulk metal. For the snapshot shown, a harmonic restraint is used to fix $\tilde{\xi} \approx 0.44$. Similarly, the cDFT constraints fix $\tilde{q} \approx 0, 1$ in the left and right panels respectively. (b) Contour plot, and (c) perspective visualization of the 2D ground-state diabatic free energy surface with thermodynamic driving force $\Delta G_{OR}^{\text{ex}} = 0$. (d) Same as (c) except setting $\Delta G_{OR}^{\text{ex}} = 1$ eV, which shifts the reduced diabat relative to the oxidized. The basins at points (0,0) and (1,1)—labeled "Ox" and "Red" in the contour plot respectively—are signatures of a CIET-like mechanism.

Electrocatalyzed CO₂ reduction is of growing interest for various industrial processes and sustainability applications [43, 44], and gold and silver electrodes are noteworthy for their high product-specificity for CO [45]. Efficient ET in this system requires the presence of cations in the solution, and the mechanism of this effect has been debated [46–48]. Recent simulation results have suggested that the cations lower the barrier for CO₂ adsorption, thus facilitating the ET [40].

Consistent with this picture, we take as our classical CV ξ the z -coordinate of the Carbon atom defined as the (negative) distance from the electrode surface, and take $|O\rangle$ and $|R\rangle$ in Eq. (1) to be the electronic states $|\text{CO}_2\rangle$ and $|\text{CO}_2^-\rangle$ respectively. Although other choices of CV are possible (e.g., the

$\Delta G_{OR}^{\text{ex}}$	$\Delta G_{\ddagger}^{\text{CV,Red}}$	$\Delta G_{\ddagger}^{\text{ET,Red}}$	$\Delta G_{\ddagger}^{\text{2D,Red}}$	$\Delta G_{\ddagger}^{\text{CV,Ox}}$	$\Delta G_{\ddagger}^{\text{ET,Ox}}$	$\Delta G_{\ddagger}^{\text{2D,Ox}}$
-0.50	0.2	1.1	1.1	0.7	2.0	1.6
0.0	0.5	1.4	1.4	0.5	1.7	1.4
0.5	0.8	1.7	1.7	0.3	1.4	1.2
1.0	1.1	2.0	2.0	0.05	1.1	1.0

TABLE I. Comparison of activation barriers (in eV) for $\text{CO}_2 \rightarrow \text{CO}_2^-$ along the minimum energy path on the *diabatic* surfaces using three approaches: (i) considering only the CV dimension (BV approach), (ii) considering only the ET coordinate (Marcus approach), and (iii) the full 2D landscape (CIET approach). Results are shown for different values of the thermodynamic driving force $\Delta G_{OR}^{\text{ex}}$. Neither 1D method consistently reproduces the barrier from the full 2D landscape.

O–C–O bond angle; see the Supplementary Material), this z -coordinate most directly captures the interfacial ion–electron coupling relevant to the CIET mechanism.

Using these definitions, we compute the diabatic free-energy surface for CO_2 redox on a gold electrode in the presence of K^+ ions (see Fig. 1(a) and the Supplementary Material for corresponding numerical details). Figure 2(b)–(d) shows contour and perspective views of the resulting free energy surface for several thermodynamic driving forces $\Delta G_{OR}^{\text{ex}}$. From Eq. (4) we obtain $(q_O, \xi_O) = (-7.0 \text{ eV}, -5.4 \text{ \AA})$ and $(q_R, \xi_R) = (6 \text{ eV}, -2.8 \text{ \AA})$, which map to the points (0, 0) and (1, 1) respectively upon nondimensionalization. The contour plot shows relative minima in both corners corresponding to the oxidized and reduced state—the signature of a CIET-like mechanism.

It is illustrative to compare the barrier height in the 2D landscape to that which would be obtained from only considering the CV or ET coordinate alone. This comparison can be done for both the reduction and oxidation directions, and for various thermodynamic driving forces $\Delta G_{OR}^{\text{ex}}$. Results of this comparison are shown in Table I. We denote by $G_{\ddagger}^{\text{CV,Red/Ox}}$ the reaction barrier that would be obtained by considering only the CV dimension, collapsing the ET dimension to the vertex of each Marcus parabolas in the manifold. We denote by $G_{\ddagger}^{\text{ET,Red/Ox}}$ the reaction barrier that would be obtained by considering only the ET dimension, taking the cross sectional Marcus parabolas at fixed CV. Finally we denote by $G_{\ddagger}^{\text{2D,Red/Ox}}$ the activation barrier obtained from the full 2D approach, which is obtained numerically from Eq. (10). Note crucially that while $G_{\ddagger}^{\text{ET,Red/Ox}}$ corresponds to a valid (although possibly higher energy) reaction path, $G_{\ddagger}^{\text{CV,Red/Ox}}$ does not correspond to a physical reaction path that satisfies the Franck Condon principle [1, 49] and is included only for illustrative purposes. We see that the CV-only approach is consistently way too small for both the reduction and oxidation directions, suggesting the importance of ET in this reaction. Though the ET-only approach is in good agreement with the full 2D approach in the reduction direction, it disagrees significantly for the oxidation direction.

Note that the evaluation of the reaction barrier at various $\Delta G_{OR}^{\text{ex}}$ provides a numerical method to evaluate the rate Eq. (18) above, and the application of this method to experimental reaction rates will be the subject of future work.

Adiabatic Corrections. The landscape presented above can

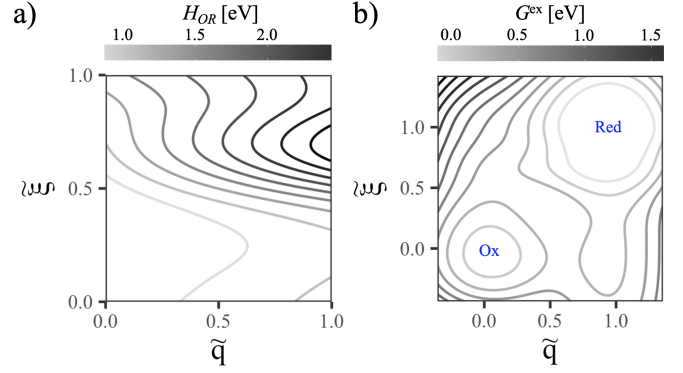


FIG. 2. (a) Contour plot of the electronic coupling H_{OR} for CO_2 redox across the 2D surface. (b) Contour plot of 2D ground-state *adiabatic* free energy surface setting $\Delta G_{OR}^{\text{ex}} = -0.2 \text{ eV}$, which corresponds to $\Delta G_{\text{eff}}^{\text{ex}} = -0.5 \text{ eV}$, characteristic of the reduction direction.

be modified when the reaction has adiabatic character, which is thought to be the case for CO_2 redox [40, 42]. In this case, if an effective coupling $H_{OR}(\tilde{q}, \tilde{\xi})$ were known, the adiabatic surface could be computed by diagonalizing the two-level system

$$G_{-}^{\text{ex}}(\tilde{q}, \tilde{\xi}, \Delta G_{OR}^{\text{ex}}) = \frac{G_O^{\text{ex}}(\tilde{q}, \tilde{\xi}) + G_R^{\text{ex}}(\tilde{q}, \tilde{\xi}, \Delta G_{OR}^{\text{ex}})}{2} - \frac{1}{2} \sqrt{((G_O^{\text{ex}}(\tilde{q}, \tilde{\xi}) - G_R^{\text{ex}}(\tilde{q}, \tilde{\xi}, \Delta G_{OR}^{\text{ex}}))^2 + 4|H_{OR}(\tilde{q}, \tilde{\xi})|^2)}. \quad (15)$$

Note that the true coupling value

$$H_{OR}(\mathbf{R}) = \langle O(\mathbf{R}) | \hat{H} | R(\mathbf{R}) \rangle \quad (16)$$

corresponding to a nuclear coordinate \mathbf{R} can be approximated from the Kohn-Sham cDFT orbitals according to Ref. [50], but will fluctuate throughout an AIMD trajectory. We can thus time average to approximate a mean coupling

$$H_{OR}(0, \tilde{\xi}) = \frac{1}{T} \int dt \int d^{3N} \mathbf{R} \delta(\tilde{\xi}(\mathbf{R}_O(t)) - \tilde{\xi}) H_{OR}(\mathbf{R}_O(t)), \quad (17a)$$

$$H_{OR}(1, \tilde{\xi}) = \frac{1}{T} \int dt \int d^{3N} \mathbf{R} \delta(\tilde{\xi}(\mathbf{R}_R(t)) - \tilde{\xi}) H_{OR}(\mathbf{R}_R(t)), \quad (17b)$$

$$H_{OR}(\tilde{q}, \tilde{\xi}) = H_{OR}(0, \tilde{\xi}) + \tilde{q}[H_{OR}(1, \tilde{\xi}) - H_{OR}(0, \tilde{\xi})], \quad (17c)$$

where T is the total time of the trajectory, assumed to be sufficiently large. In Eq. (17) We have first averaged along the minima in the CV direction and then employed a linear interpolation to approximate the coupling for values $0 < \tilde{q} < 1$. In this case, as discussed in Ref. [16], the corresponding adiabatic rate expression differs only by the prefactor

$$k^{\text{adiabatic}} = \frac{k_B T}{h} \int d\epsilon_R \rho(\epsilon_R) n(\epsilon_R) \exp\left(-\frac{\Delta G_{\ddagger}^{\text{ex}}(\Delta G_{OR}^{\text{ex}}, \epsilon_R)}{k_B T}\right). \quad (18)$$

$\Delta G_{\text{eff}}^{\text{ex}}$	$\Delta G_{\text{OR}}^{\text{ex}}$	$\Delta G_{\ddagger}^{\text{CV,Red}}$	$\Delta G_{\ddagger}^{\text{ET,Red}}$	$\Delta G_{\ddagger}^{\text{2D,Red}}$	$\Delta G_{\ddagger}^{\text{CV,Ox}}$	$\Delta G_{\ddagger}^{\text{ET,Ox}}$	$\Delta G_{\ddagger}^{\text{2D,Ox}}$
-0.5	-0.2	0.3	0.4	0.4	0.8	1.4	0.9
0.0	0.4	0.5	0.8	0.5	0.5	0.9	0.5
0.5	0.9	0.7	1.3	0.7	0.1	0.5	0.2
1.0	1.5	1.0	1.8	1.0	0.0	0.0	0.0

TABLE II. Same as Table I, except using the ground-state *adiabatic* surface, and adjusting $\Delta G_{\text{OR}}^{\text{ex}}$ to obtain the desired $\Delta G_{\text{eff}}^{\text{ex}}$.

Figure 2(a) shows a contour plot of the electronic coupling across the full 2D landscape, while Fig. 2(b) shows a contour plot of the computed adiabatic free energy surface adjusted according to Eq. (15). Note that the coupling values are quite large—on the order of 1–3 eV—consistent with the theoretical prediction of Ref. [16].

To calculate the TS, we note that in the adiabatic case, the TS is not confined to occur within the set \mathcal{J} defined in Eq. (9), and so the restriction in the minimization in Eq. (10a) must be lifted. We therefore located the TS using a minimax (lowest-saddle) search, in which all neighboring grid points were connected by edges weighted by the higher of their energies, and the smallest edge-maximum path connecting the bottom-left and top-right minima was located via a Kruskal-style union-find algorithm [51]. Furthermore, note that in contrast to the non-diabatic approximation above, the experimentally observed driving force $\Delta G_{\text{eff}}^{\text{ex}}$ is no longer strictly equivalent to the diabatic shift $\Delta G_{\text{OR}}^{\text{ex}}$, so the latter must be adjusted analyze the former [16].

The resulting energy barriers are reported in Table II. We observe that many of the barriers are significantly lower com-

pared to the diabatic landscape, and notably barrierless transition is obtained at an overpotential not predicted in the non-diabatic case. Furthermore, both in both the reduction and oxidation directions, there is no consistent agreement between the barriers calculated from either 1D approach and the full 2D landscape. These results provide evidence that the multidimensional, adiabatic-corrected approach presented in this Letter is necessary to accurately compute ET barrier heights in general.

In conclusion, we have introduced a general framework for constructing the 2D free energy surface of an ET reaction coupled to a classical CV in terms of constrained *ab initio* trajectories, which can be improved along with sampling efficiency and accurate simulation of diabatic states. Applied to an example reaction of CO₂ redox, we showed that the activation barrier computed either using the ET coordinate or CV alone can be significantly misleading. Although further sampling is needed to resolve the CV-dependence of the reorganization energy, our framework readily accommodates such dependence and would be expected to yield even larger deviations from the Marcus picture. We expect that the coupled-electron transfer view presented in this Letter will provide a more accurate perspective on the activation of a wide class of electron transfer reactions in anisotropic or interfacial environments.

Acknowledgements. This work was supported by the MIT Faculty Research Innovation Fund (FRIF) through the generosity of Irv and Melinda Simon. E.A. is grateful to Ezra Alexander, Mohammadhasan Dinpajoo, Beck Hanscam, Ziyue Jiang, Matthias Kick, Abraham Nitzan, Leah Weisburn, Junghyun Yoon, and Chao Zhang for useful discussions.

-
- [1] R. A. Marcus, *J. Chem. Phys.* **24**, 966–978 (1956).
[2] R. A. Marcus, *Annu. Rev. Phys. Chem.* **15**, 155–196 (1964).
[3] N. S. Hush, *Trans. Faraday Soc.* **57**, 557 (1961).
[4] M. Tachiya, *J. Phys. Chem.* **93**, 7050 (1989).
[5] A. Warshel and M. Levitt, *J. Mol. Biol.* **103**, 227 (1976).
[6] J. Blumberger, *Chem. Rev.* **115**, 11191 (2015).
[7] M. Z. Bazant, *Faraday Discuss.* **246**, 60 (2023).
[8] D. Fraggedakis, M. McEldrew, R. B. Smith, Y. Krishnan, Y. Zhang, P. Bai, W. C. Chueh, Y. Shao-Horn, and M. Z. Bazant, *Electrochim. Acta* **367**, 137432 (2021).
[9] R. I. Cukier and D. G. Nocera, *Annu. Rev. Phys. Chem.* **49**, 337 (1998).
[10] S. Hammes-Schiffer and A. V. Soudackov, *J. Phys. Chem. B* **112**, 14108 (2008).
[11] J. Halldin Stenlid, P. Žgunc, D. Vivona, A. Aggarwal, K. Gordiz, Y. Zhang, S. Pathak, M. Z. Bazant, Y. Shao-Horn, A. Baskin, and J. W. Lawson, *ACS Energy Lett.* **9**, 3608 (2024).
[12] Y. Zhang, D. Fraggedakis, T. Gao, S. Pathak, D. Zhuang, C. Grosu, Y. Samantaray, A. R. C. Neto, S. R. Duggirala, B. Huang, Y. G. Zhu, L. Giordano, R. Tataru, H. Agarwal, R. M. Stephens, M. Z. Bazant, and Y. Shao-Horn, *Science* **390**, eadq2541 (2025).
[13] H. Zhao, H. D. Deng, A. E. Cohen, J. Lim, Y. Li, D. Fraggedakis, B. Jiang, B. D. Storey, W. C. Chueh, R. D. Braatz, and M. Z. Bazant, *Nature* **621**, 289 (2023).
[14] R. W. Gurney and E. Rutherford, *Proc. R. Soc. Lond. A* **134**, 137 (1931).
[15] J. A. V. Butler, *Proc. R. Soc. Lond. A* **157**, 423–433 (1936).
[16] E. Abraham, J. Yoon, T. V. Voorhis, and M. Z. Bazant, arXiv (2025), submitted on 13 Oct 2025, arXiv:2510.10996 [quant-ph].
[17] *J. Electroanal. Chem.* **735**, 77 (2014).
[18] C. E. D. Chidsey, *Science* **251**, 919 (1991).
[19] A. Nitzan, *Chemical Dynamics in Condensed Phases: Relaxation, Transfer, and Reactions in Condensed Molecular Systems* (Oxford University Press, 2006).
[20] H. Bässler, *Phys. Status Solidi B* **175**, 15 (1993).
[21] C. Jarzynski, *Phys. Rev. Lett.* **78**, 2690 (1997).
[22] G. Bussi, A. Laio, and M. Parrinello, *Phys. Rev. Lett.* **96**, 090601 (2006).
[23] A. Barducci, G. Bussi, and M. Parrinello, *Phys. Rev. Lett.* **100**, 020603 (2008).
[24] A. Musaelian, S. Batzner, A. Johansson, L. Sun, C. J. Owen, M. Kornbluth, and B. Kozinsky, *Nat. Commun.* **14**, 579 (2023).
[25] S. Batzner, A. Musaelian, L. Sun, M. Geiger, J. P. Mailoa, M. Kornbluth, N. Molinari, T. E. Smidt, and B. Kozinsky, *Nat. Commun.* **13**, 2453 (2022).
[26] O. T. Unke, S. Chmiela, M. Gastegger, K. T. Schütt, H. E. Sauceda, and K.-R. Müller, *Chem. Rev.* **121**, 10142 (2021).
[27] T. Van Voorhis, T. Kowalczyk, B. Kaduk, L.-P. Wang, C.-L. Cheng, and Q. Wu, *Annu. Rev. Phys. Chem.* **61**, 149 (2010).
[28] B. Kaduk, T. Kowalczyk, and T. Van Voorhis, *Chem. Rev.* **112**, 137 (2012).

- 321 (2012).
- [29] Q. Wu and T. Van Voorhis, *Phys. Rev. A* **72**, 024502 (2005).
- [30] C. S. Ahart, K. M. Rosso, and J. Blumberger, *J. Chem. Theory Comput.* **18**, 4438 (2022).
- [31] N. Holmberg and K. Laasonen, *J. Chem. Theory Comput.* **13**, 587 (2017).
- [32] M. Melander, E. Ö. Jónsson, J. J. Mortensen, T. Vegge, and J. M. García Lastra, *J. Chem. Theory Comput.* **12**, 5367 (2016).
- [33] A. Warshel, *J. Phys. Chem.* **86**, 2218 (1982).
- [34] A. Warshel and P. W. W., *Q. Rev. Biophys.* **34**, 563–679 (2001).
- [35] Formally, the free energy used in this work is the excess free energy G^{ex} , which retains only the terms that affect the potential experienced by an individual particle, subtracting off the.
- [36] M. Sprik and G. Ciccotti, *J. Chem. Phys.* **109**, 7737 (1998).
- [37] G. Bussi, A. Laio, and M. Parrinello, *Phys. Rev. Lett.* **96**, 090601 (2006).
- [38] Interestingly, if we assume the energy gap sampling (Eq. (1)) is harmonic, equating the change in free energy between the minima of the Marcus parabola at a particular value of the CV implies that $U_R^{\text{bias}}(\xi) - U_O^{\text{bias}}(\xi) = \frac{1}{2}(E_O(q|\xi) + E_R(q|\xi) - \lambda_R(\xi) + \lambda_O(\xi))$. This equation relates the ET-coordinate statistics to the CV statistics, although in practice, it may not hold exactly due to asymmetry/anharmonicity in the ET, sampling insufficiency, or methodological uncertainty.
- [39] P. Hänggi, P. Talkner, and M. Borkovec, *Rev. Mod. Phys.* **62**, 251 (1990).
- [40] X. Qin, H. A. Hansen, K. Honkala, *et al.*, *Nat. Commun.* **14**, 7607 (2023).
- [41] B. A. Zhang, C. Costentin, and D. G. Nocera, *The Journal of Chemical Physics* **153**, 094701 (2020).
- [42] M. T. M. Koper, *J. Solid State Electrochem.* **28**, 1601 (2024).
- [43] Z. W. Seh, J. Kibsgaard, C. F. Dickens, I. Chorkendorff, J. K. Nørskov, and T. F. Jaramillo, *Science* **355**, 4998 (2017).
- [44] S. Nitopi, E. Bertheussen, S. B. Scott, X. Liu, A. K. Engstfeld, S. Horch, B. Seger, I. E. L. Stephens, K. Chan, C. Hahn, J. K. Nørskov, T. F. Jaramillo, and I. Chorkendorff, *Chem. Rev.* **119**, 7610 (2019).
- [45] Y. Hori, A. Murata, K. Kikuchi, and S. Suzuki, *J. Chem. Soc., Chem. Commun.*, 728 (1987).
- [46] J. Resasco, L. D. Chen, E. Clark, C. Tsai, C. Hahn, T. F. Jaramillo, K. Chan, and A. T. Bell, *J. Am. Chem. Soc.* **139**, 11277 (2017).
- [47] S. Ringe, E. L. Clark, J. Resasco, A. Walton, B. Seger, A. T. Bell, and K. Chan, *Energy Environ. Sci.* **12**, 3001 (2019).
- [48] F. Zhang and A. C. Co, *Angew. Chem. Int. Ed.* **59**, 1674 (2020).
- [49] W. F. Libby, *The Journal of Physical Chemistry* **56**, 863 (1952).
- [50] Q. Wu and T. Van Voorhis, *The Journal of Chemical Physics* **125**, 164105 (2006).
- [51] J. B. Kruskal, *Proceedings of the American Mathematical Society* **7**, 48 (1956).